Synthetic Metals 217 (2016) 144–151

Contents lists available at ScienceDirect

Synthetic Metals

journal homepage: www.elsevier.com/locate/synmet

Fatigue in organic semiconductors: Spectroscopic evolution of microstructure due to cyclic loading in poly(3-heptylthiophene)

Adam D. Printz, Andrew S.-C. Chiang, Suchol Savagatrup, Darren J. Lipomi*

Department of NanoEngineering, University of California, San Diego, 9500 Gilman Drive, Mail Code 0448, La Jolla, CA 92093-0448, USA

ARTICLE INFO

Article history:
Received 7 November 2015
Received in revised form 25 February 2016
Accepted 23 March 2016
Available online xxx

Keywords:
P3HpT
Stretchable electronics
Stretchable solar cells
Conjugated polymer
Mechanical properties
Organic semiconductor

ABSTRACT

Organic electronic materials have many characteristics that make them attractive for applications in which mechanical deformability—i.e., flexibility and stretchability—are required. While deformation often degrades the performance of these devices, very little is known about the effects of cyclic loading —i.e., mechanical fatigue—on the microstructure and mechanical properties of the active materials. This paper examines the evolution of microstructure, stiffness, and ductility of thin films of poly (3-heptylthiophene) (P3HpT) as the film undergoes cyclic straining using ultraviolet-visible (UV–vis) spectroscopy and film-on-elastomer techniques. Thin films of P3HpT are cyclically stretched by 5, 10, or 25 percent (i.e., below, at, and above the yield point—the point at which the polymer plastically deforms with strain) up to 10000 cycles. UV–vis absorption spectroscopy is taken in intervals and the weakly interacting H-aggregate model is used to determine the aggregate quantity (from the vibronic progression) and quality (from the exciton bandwidth) in the films. Films cyclically strained at 5 and 10 percent (below and at the yield point) do not undergo significant reduction in the aggregated fraction of polymer chains, while films strained to 25% (above the yield point) undergo a reduction in aggregated fraction of over 10% by the 2000th cycle. At 25% strain, a significant reduction in the buckling wavelength from $3.4 \pm 0.4\ \mu m$ to $2.4 \pm 0.3\ \mu m$ is observed within the first 100 strain cycles suggesting a significant reduction in the stiffness and resilience of the films. A significant decrease in ductility is observed in films cyclically strained, and the effect is found to increase with increasing levels of strain. These results suggest that materials cyclically strained below their yield point will retain a microstructure that is their most electronically favorable, and that the mechanical properties of materials strained above their yield point will evolve significantly under repeated deformation. This information can be used to inform design where accommodation of repetitive strain is required, such as outdoor, portable, and wearable devices.

1. Introduction

Organic electronic devices have several key advantages over their inorganic counterparts, including low cost [1–3], manufacturability by roll-to-roll processes [4–6], molecular customizability [7,8], and their flexibility or stretchability—qualities that (though often assumed) are not always present [9–11]. These properties could enable devices in a new range of new applications including wearable [12–14] and implantable biosensors [15,16], electronic skins [17,18], and mechanically robust organic photovoltaics that can handle harsh outdoor environments [11,19,20]. Many of these applications require materials capable of handling repetitive strains. For example, as part of the "Lighting Africa" initiative, lamps powered by flexible OPVs were deployed to rural Africa; these lamps and flexible organic photovoltaic (OPV) devices were subjected to the repeated mechanical stresses of everyday use [21]. After only three weeks of testing, it was found that 40% of the devices suffered catastrophic mechanical failure, attributed to contact failure [21]. While it is expected that the failure due to contacts will be resolved, it highlights an area of the field that requires further understanding: how devices behave when repeatedly strained. It is thus important to understand how the microstructure of semiconducting layers of devices evolves under cyclic loading. Ideally, the semiconducting materials selected for a device will be able to accommodate the strain elastically so that no permanent deformation of the active components of the device occurs. However, under cyclic strain, even devices that accommodate the strain elastically might deform irreversibly with continued cycling. Prior to catastrophic failure of devices such as organic solar cells and thin-film transistors due to cracking, changes in the

* Corresponding author.
E-mail address: dlipomi@eng.ucsd.edu (D.J. Lipomi).

http://dx.doi.org/10.1016/j.synthmet.2016.03.033
0379-6779/

morphology of the active materials could produce changes in the electronic structure of the material, which may be deleterious to the performance of devices.

Fatigue is a phenomenon in materials science whose effects are well known to be deleterious. In metals, strain hardening due to the accumulation of dislocations causes embrittlement and eventual structural failure. In conventional polymers, accommodation of cyclic strains dissipates heat that can produce chain scission and the rearrangement of microstructure that both have the effect of reducing the load-bearing capacity of a structure. In the context of semiconducting polymers, the effect of repetitive loading has not been explored but should almost certainly have an effect on the microstructure and thus the electronic structure. We thus explored the effect of the repetitive strain on the microstructure of thin films of the polymer poly(3-heptylthiophene) (P3HpT) (Fig. 1). We measured the absorption of relaxed films after straining and used the weakly interacting H-aggregate model developed by Spano and others to evaluate the evolution of the fraction of polymer aggregates and the order within these aggregates, as manifested in the exciton bandwidth [22–25]. We expected that as the number of cycles of strain increased, the aggregation would decrease, which would be concomitant with a decrease in the amount of energy needed to deform the film (i.e., reduced modulus and resilience). We observed different behavior for films cycled below, at, and above the yield point of P3HpT (using a value of yield point previously measured by our group) [26].

2. Experimental design

2.1. Selection of materials

Poly(3-heptylthiophene) was selected as the conjugated polymer to be analyzed because of its favorable electronic and mechanical properties [27,28]. We previously reported that, when mixed with [6,6]-phenyl-C61-butyric acid methyl ester ($PC_{61}BM$) in organic photovoltaic devices with all stretchable components, the power conversion efficiency (PCE) of devices made from P3HpT was $2.16 \pm 0.17\%$, similar to that of P3HT devices ($2.04 \pm 0.27\%$) [27]. In addition to good photovoltaic performance, P3HpT had a tensile (or Young's) modulus of 0.07 ± 0.01 GPa, which was an order of magnitude lower than P3HT (1.09 ± 0.15 GPa). Moreover, the crack-onset strain of the films on elastic substrates was significantly greater for P3HpT (58%) than for P3HT (10%) [27]. Conveniently, all members of the family of poly(3-alkylthiophene)s (P3ATs) form thin films with aggregates that can be modeled by the weakly interacting H-aggregate model [22,25]. Polydimethylsiloxane (PDMS) was selected as the elastomeric substrate because it is transparent to visible light and therefore allowed measurement of the absorption spectra of our films over the wavelengths of interest (300–850 nm).

2.2. Weakly interacting H-aggregate model

The stiffness of thin films of the poly(3-alkylthiophene) (P3AT), poly(3-hexylthiophene) (P3HT) has been correlated to the order present in the films [25,29]. In the aggregated state, the coupled electron-vibrational (vibronic) transitions determine the absorption of weakly interacting H-aggregates. Spano and others developed the weakly interacting H-aggregate model, which models the absorption by aggregated states in polymer films that form H-aggregates as Gaussian fits by: [22–25]

$$A(E) \propto \sum_{m=0} \left(\frac{S^m}{m!}\right) \times \left(1 - \frac{We^{-S}}{2E_p} \sum_{n \neq m} \frac{S^n}{n!(n-m)}\right)^2 \times \exp\left(\frac{-(E - E_{00} - mE_p - \frac{1}{2}WS^m e^{-S})^2}{2\sigma^2}\right) \quad (1)$$

where A is the absorption by an aggregate as a function of the photon energy (E). W is the free exciton bandwidth, which is related to the nearest neighbor interchain excitonic coupling. Upon coupling, a dispersion of the energies occurs, the width of which is equal to W (which is four times the nearest neighbor coupling) [30]. E_{00} is the energy of the $0 \rightarrow 0$ vibronic transition, which is allowed assuming some disorder in the aggregates [22]. S is the Huang–Rhys factor, which is calculated from absorption and emission spectra, and is set to 1 for P3ATs [22,23]. E_p is the intermolecular vibration energy, which (in the case where $S = 1$) is set to 0.179 eV as determined by Raman spectroscopy [31]. The terms m and n are the ground- and excited- state vibrational levels, and σ is the Gaussian line width. The Gaussian line width, σ, E_p, W, and the scaling factor for the calculated absorption were found by a least-squares fit to the experimental absorption in the region of 550–620 nm (2.25–2.00 eV) [24,25,32]. This range was selected because in it the absorption is dominated by the polymer aggregates, while above 540 nm (2.30 eV), the amorphous polymer dominates absorption [23,32].

2.3. Cyclic loading of P3HpT

To understand the evolution of the microstructure of thin films of P3HpT as they are strained cyclically, we measured the absorption spectra before straining, as well as after 1, 10, 20, 50, 100, 200, 500, 1000, 2000, 5000, and 10000 strain cycles while the

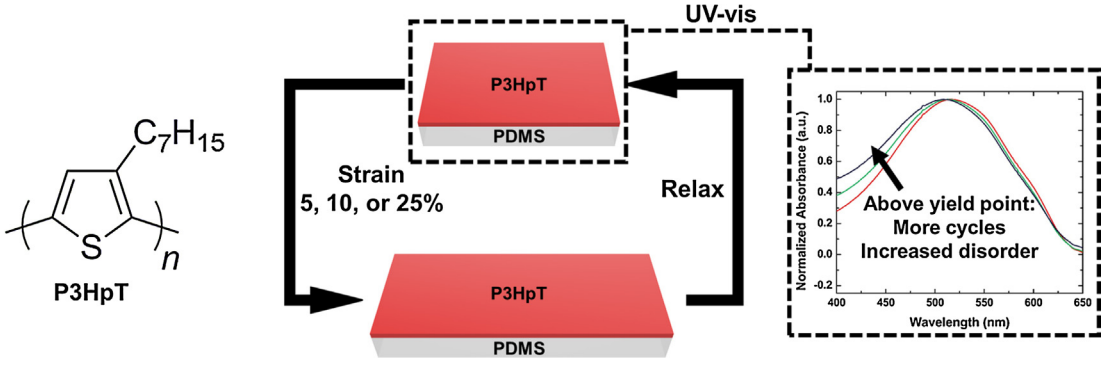

Fig. 1. Thin films of poly(3-heptylthiophene) (P3HpT) were transferred to elastomeric substrates of polydimethylsiloxane (PDMS) and strained cyclically 5%, 10%, or 25%. To evaluate the evolution of their microstructure, absorption spectra were taken periodically and the weakly interacting H-aggregate model was fit to the data.

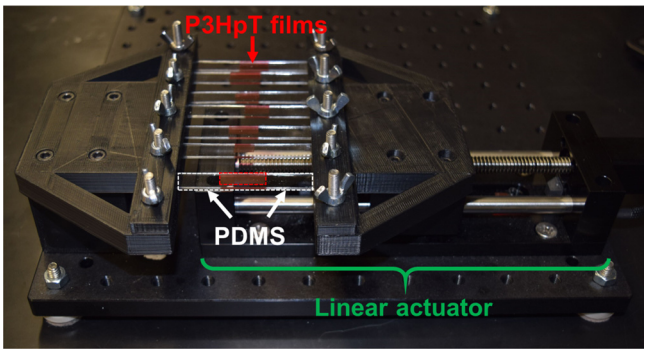

Fig. 2. Photograph of the stretch apparatus stretching P3HpT thin films on PDMS substrates.

films were in the relaxed state. Seven samples were strained simultaneously using a purpose-built apparatus (Fig. 2). We then applied the weakly interacting H-aggregate model to these spectra to determine the quantity and quality of aggregation in the films. We also wanted to understand the effects on microstructure of cyclic straining below, at, and above the yield point. In P3HpT, the yield point was previously determined to be $11.3 \pm 1.5\%$, so we chose to cyclically strain the films 5, 10, and 25% [26]. We anticipated the greatest changes in microstructure would occur above the yield point, while lower changes would occur near the yield point, and almost no change would occur below the yield point.

3. Results and discussion

The absorption spectra of P3HpT after increasing cycles of strain are shown in Fig. 3. The strongly absorbing region by the aggregates in the films are between 550 and 620 nm, and shoulder features—i.e., vibronic transitions—were clearly observable in this region for all of the samples before strain had been applied. The ratio of the magnitude of the $0 \rightarrow 0$ (the shoulder at 605 nm) and $0 \rightarrow 1$ (the shoulder at 550 nm) vibronic transitions is associated with local ordering (specifically the conjugation length) in the aggregates [22,23,25]. While a large change in the vibronic peaks was not observable in the films cyclically strained 5% (Fig. 3a), a reduction in the vibronic peaks was observable in films cyclically strained 10% (Fig. 3b) and 25% (Fig. 3c). (Fits of the weakly interacting H-aggregate model to the experimental absorption spectra are available in Figs. S1–S3.) The decrease in the vibronic peaks is indicative of a decrease in the quality (or local ordering) of the aggregates. At wavelengths below 540 nm, the amorphous polymer is more strongly absorbing. In the films that have been cyclically strained 25%, there is a significant increase in the absorbance below 500 nm as the number of strain cycles increases. This increase in the absorption at lower wavelengths suggests that there is a decrease in the quantity of aggregates—or an increase in the quantity of disordered or amorphous regions—in the film. The increase in disorder is consistent with the possibility of plastic deformation in the film with repetitive strain.

Next, we probed the evolution of the microstructure by applying the weakly interacting H-aggregate model to the absorption spectra (Fig. 4). To account for sample-to-sample variations, the fraction of aggregates were normalized to the samples before they underwent any strain (i.e., 0 cycles). These values were plotted against the number of strain cycles in Fig. 4a. Additionally, to account for oxidative degradation, a control sample that was not cyclically strained was made and measured at the same time as those samples that were cyclically strained. The aggregate fraction and W were also calculated for these controls and normalized to the values determined from the absorption spectra taken at the same time as the samples before they were strained (i.e., 0 cycles, Figs. S4). The deviation of the normalized aggregate fraction and W from unity—assuming no oxidation or other environmental factors, the parameters should remain constant and equal to unity—were then subtracted from the data of the cyclically strained samples. A small decrease in aggregation

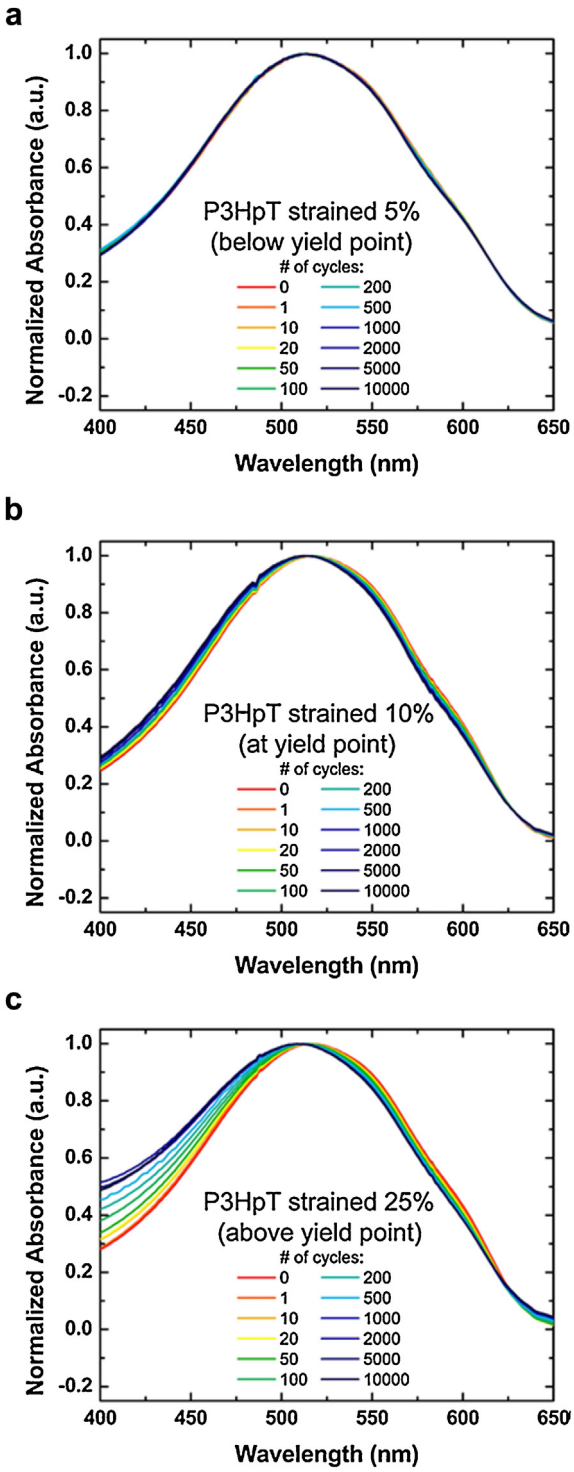

Fig. 3. Absorption spectra of P3HpT thin films undergoing cyclic strain. (a) Thin films strained below the yield point of P3HpT (all curves essentially overlap). (b) Thin films strained near the yield point of P3HpT. (c) Thin films strained above the yield point of P3HpT.

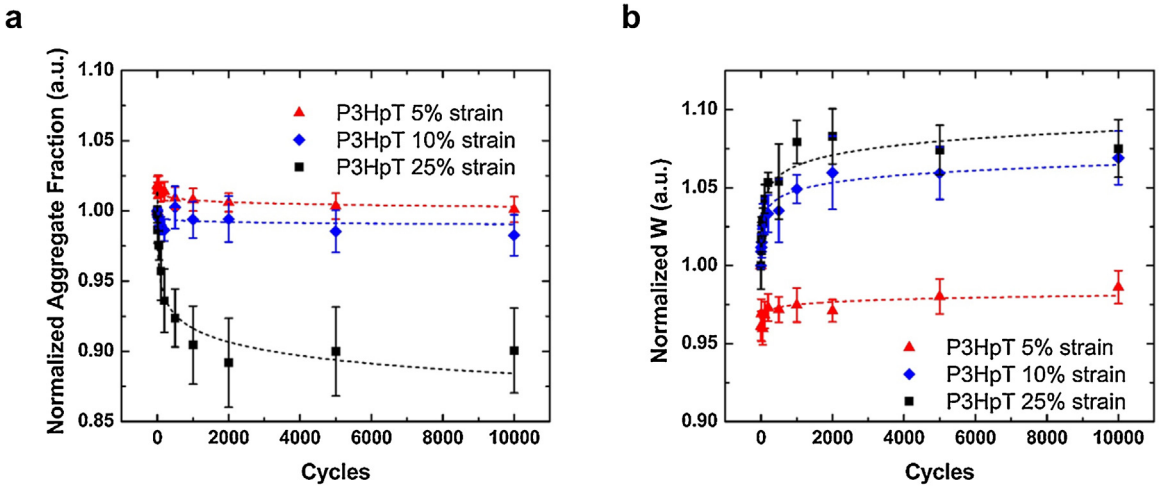

Fig. 4. Weakly interacting H-aggregate model parameters for the cyclically strained films. (a) The fraction of aggregates in the films normalized to the amount of aggregation initially present. The aggregation was measured only between 400 and 650 nm, therefore the contribution to absorbance by the amorphous material is underestimated. (b) The exciton bandwidth, W, normalized to the initial values. W is inversely related to the average conjugation length of the polymer, and is therefore an indicator of aggregate order. The dotted lines represent exponential fits for the data from 1 cycle to 10000 cycles.

was observed in the samples cyclically strained 5 and 10%, while a much greater decrease in aggregation was observed in samples cyclically strained 25%. It should be noted that while the normalized aggregate fraction values for the samples strained 5% increase to above 1.0, it is likely an artifact due to subtracting out the deviation of the control from unity. In all cases, the disruption in aggregation that occurred appeared to slow down once the samples had undergone 2000 strain cycles. This observation suggests that most degradation due to microstructural evolution in conjugated polymers is likely to saturate—for P3HpT saturation occurs around 2000 cycles.

The exciton bandwidth, W, is inversely related to conjugation length and provides information about the local ordering (or quality) of the polymer aggregates. The exciton bandwidth was normalized to the samples at 0 cycles (with the deviation from unity for the normalized control subtracted out to account for any oxidative effects) for 5, 10, and 25% strain plotted against the number of cycles is shown in Fig. 4b. We observed that W in the samples strained 5% does not change significantly, indicating little change in the quality of aggregates and in the conjugation length. However, at 10% and 25% strain, the W values increased, indicating a decrease in the conjugation length of the polymer in the aggregates. The decrease in the conjugation length at 25% is unsurprising and is consistent with the observation of decreased aggregation. However, the decrease in conjugation length of the samples cyclically strained at 10% is surprising because it is not coupled with a decrease in aggregate quantity. One possible explanation for this observation is that there is a critical amount of local disorder that must occur in aggregates because they become completely disrupted.

Micrographs of the P3HpT films after 0, 1, 10, and 10,000 strain cycles are shown in Fig. 5. The films strained at 5%—below the yield point—showed little evidence of plastic deformation (i.e., buckling of the film was barely detectable—i.e., low-amplitude—by optical microscopy above 10 cycles), although some delamination was evident at 5000 cycles. These observations are consistent with the absorption spectra and H-aggregate parameters, which suggest minimal microstructural evolution. When the cyclic strain was increased to 10%—near the previously reported yield point of P3HpT [26]—the films developed surface buckles by 10 cycles, although the buckles were again very faint in the micrograph. While the buckling did not become more evident with increased cycling at 10% strain, delamination occurred in a few samples by 2000 cycles and in all by 5000 cycles. A much more dramatic effect occurred for the films cyclically strained 25%, which was above the yield point of P3HpT [26]. Buckling of the film was observed after the first cycle, and the buckles became more pronounced (i.e., higher amplitude) by 10 cycles. By 5000 cycles, significant delamination was observed. The significant buckling and delamination at 25% strain was consistent with the plastic deformation (and associated decrease in aggregate quantity and quality) suggested by the absorption spectra and H-aggregate parameters for these samples. We believe the micrographs, absorption spectra, and H-aggregate results point to an important design parameter for devices expected to undergo cyclic straining, the material yield point. The cyclic straining of the samples at or below the material yield point were much less disruptive to the film aggregation than that the samples strained above the yield point (although the W of the samples at the yield point increased considerably), suggesting that in applications where repetitious strain is required, selection of materials which have a yield point higher than the anticipated strain are likely to undergo only minor changes in microstructure.

To determine if the evolution of microstructure was correlated with a change in mechanical properties, we measured the buckling wavelength of the films cyclically strained 25% after various cycles (Fig. 6). (The samples strained 25% were selected because they featured the most prominent buckling.) Under ideal conditions —i.e., small compressive strains, $\leq$5%, and a purely elastic film—the buckling wavelength is correlated to the tensile modulus because it is dependent on an energy balance between deforming the underlying soft substrate and bending the relatively rigid film [33]. Using this effect, Stafford et al. developed a buckling-based metrology to determine the tensile modulus of thin films [34]. The tensile modulus is correlated with the buckling wavelength, meaning stiffer films have a longer buckling wavelength, and more compliant films have a shorter buckling wavelength [34–36]. We found that the buckling wavelength was the highest after the first strain cycle ($3.4 \pm 0.4\,\mu m$) and it dropped considerably to $2.8 \pm 0.5\,\mu m$ by the 10th cycle. By the 100th strain cycle, the buckling wavelength was $2.4 \pm 0.3\,\mu m$ and remained relatively constant with an increasing number of cycles. This data agreed with previous literature—and the UV–vis analysis in this study

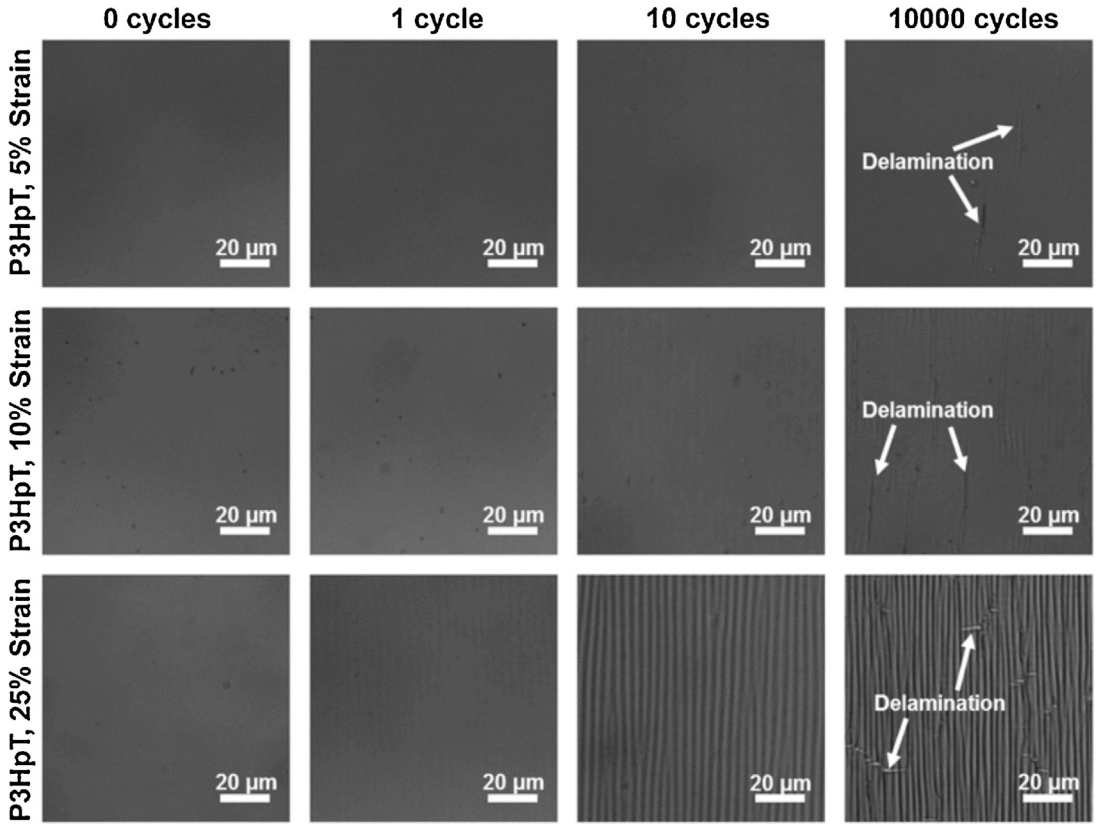

Fig. 5. Micrographs of the cyclically strained P3HpT films. Barely detectable—i.e., very low amplitude—buckling occurred in the films strained below the yield point (although delamination occurred after many cycles). At strain near the yield point, buckling occurred by 10 cycles, and at strain above the yield point, buckling occurred on the first cycle. Delamination occurred in all samples by 10000 cycles.

—that reported a decrease in stiffness (i.e., decrease in tensile modulus) with decreasing fraction of aggregated polymer chains and order [25,29], and suggests that the films became more compliant as they were cyclically strained (at least for the first few hundred strain cycles).

We were unable to quantify the precise reduction in modulus due to cycling and indicated by the decrease in buckling wavelength for two reasons. (1) The buckling methodology of Stafford et al. is valid only for small compressive strains (i.e., less than about 5%) [34]. In our experiments, a total strain of 25% of a material with a yield point of about 10% would elongate the material plastically by 15%, and thus produce a compressive strain of 15%—too large for analysis by the buckling methodology—when the film and substrate was returned to equilibrium. (2) Analysis by the method of Stafford et al. would require that no plastic deformation occurs after the first cycle of strain, which cannot be granted automatically, especially in light of the microstructural evolution indicated by UV–vis spectroscopy [34]. Ideally, to determine the tensile modulus of a thin film using the buckling methodology, the conditions of low strain (<10%), a much stiffer (and thinner) thin film than the substrate, a buckling amplitude much smaller than the wavelength, and no yielding of the thin film should be met [34]. An illustration of the microstructural evolution of P3HpT strained cyclically above its yield point is shown in Fig. 7. The quantity and quality of the aggregates in the as-cast films are disrupted after repetitive strain. This decrease in aggregate quality and quantity results in a film with a much lower tensile modulus.

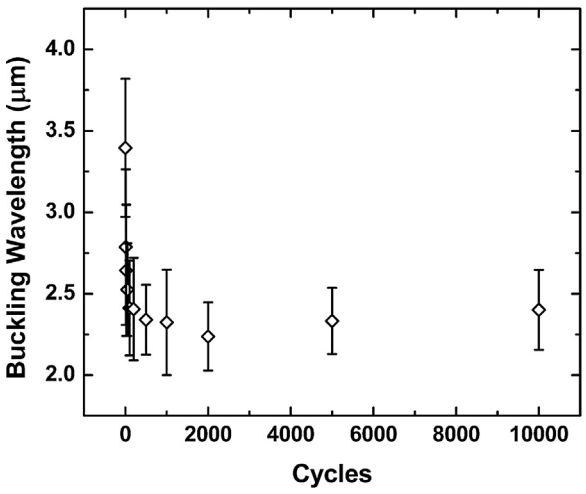

Fig. 6. The buckling wavelength versus number of cycles for P3HpT samples cyclically strained 25%. The decrease in buckling wavelength is indicative of a lower tensile modulus.

In thin films, the difference in crack features is attributable to differences in film ductility [25]. We examined the influence of the cyclic straining on the ductility of the P3HpT thin films by observing their crack features by optical microscopy. Films which had not undergone cyclic straining exhibited pinhole fracture around 90% strain (which was just below the strain at which the PDMS failed). Conversely, films which had been cyclically strained for 10000 cycles demonstrated catastrophic brittle failure. Additionally, as the strain at which films were cycled was increased, so too was the apparent brittleness of the resulting

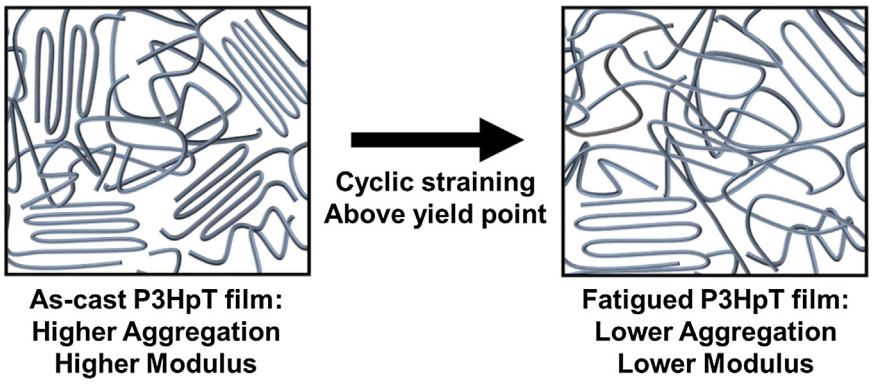

Fig. 7. An illustration demonstrating the disruption of aggregation in thin films of P3HpT cyclically strained above its yield point.

films. Micrographs of sample films strained 90% are shown in Fig. 8. To better understand the extent of the increase in brittleness, we measured the percentage of the micrographs which were occupied by cracks (or rather unoccupied by the polymer film). At 90% strain, the films cyclically strained 5%, had $5 \pm 1\%$ of the film area occupied by cracks. Films cyclically strained 10% had an area occupied by cracks of $26 \pm 2\%$, and those films cyclically strained 25% had an area occupied by cracks of $48 \pm 6\%$. The jump in crack area from the samples cyclically strained at 5% to those strained at 10% is by a factor of 5, suggesting there is a distinct embrittling of the films.

4. Conclusion

This paper described the evolution of microstructure in P3HpT with increasing cycles of strain below, at, and above the thin film yield point using the weakly interacting H-aggregate model. Experimental evidence showed that disruption of aggregation is negligible when films are cycled at strains below or near the material yield point (although the quality of the aggregates decreased with cycling at the yield point). However, when the films are cycled at strains above the yield point, significant disruption of aggregates occurs. We also observed that the majority of microstructural evolution at a single strain occurs within the first 2000 strain cycles, meaning that the degradation of electronic performance due to microstructural degradation will likely saturate. Importantly, we found that—in the samples strained above the yield point—the buckling wavelength decreased as the number of strain cycles increased, suggesting a material that became less stiff as it was cyclically strained. While the materials became less stiff, catastrophic failure through brittle fracture was observed in samples cyclically strained 10000 times. This behavior is undesirable for devices and thus reducing the brittleness of organic films that undergo cyclic strain certainly warrants further study. Our findings highlight the yield point as an important figure of merit for devices used in applications where repetitive strain is expected, such as outdoor, portable, and wearable devices.

5. Experimental methods

5.1. Materials

Poly(3-heptylthiophene) (P3HpT, $M_n = 35$ kDa, PDI = 1.5, regioregularity = 93.6%) was purchased from Rieke Metals, Inc., and used as received. PDMS, Sylgard 184 (Dow Corning), was prepared according to the manufacturer's instructions at a ratio of 10:1 (base:crosslinker) and cured at 75 °C for 25 min before it was used for mechanical testing. (Tridecafluoro-1,1,2,2-tetrahydrooctyl)-1-trichlorosilane (FOTS) was obtained from Gelest. Chloroform, acetone, and isopropyl alcohol (IPA) were obtained from Sigma-Aldrich and used as received.

5.2. Preparation of samples for testing

Glass slides were cut into squares (2.5 cm × 2.5 cm) with a diamond-tipped scribe. They were then subsequently cleaned with Alconox solution (2 mg mL^{-1}), deionized water, acetone, and then isopropyl alcohol (IPA) in an ultrasonic bath for 10 min each and then rinsed and dried with compressed air. Next, the glass was plasma treated at ~30 W for 3 min at a base pressure of 200 mtorr ambient air to remove residual organic material and activate the

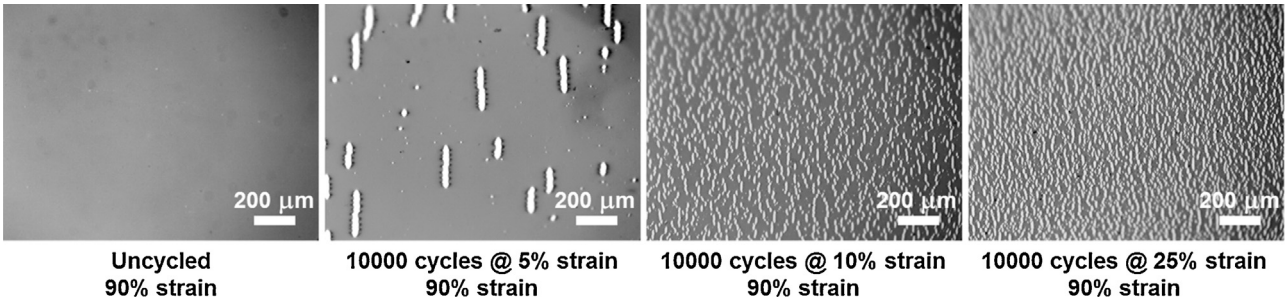

Fig. 8. Micrographs of the cracking in P3HpT films under different strain cycling conditions. All micrographs were taken at 90% strain (the highest strain before failure of the substrates) to demonstrate that while only pinhole cracks were observable in the uncycled films, brittle fracture occurred in films that had been cyclically strained. Additionally, as the strain at which the films were cycled increased, so too did the density of the cracks in the films.

surface. The slides were then placed in a vacuum desiccator with a glass vial containing ~100 μL of FOTS and put under house vacuum for a minimum of 3 h to passivate the surface. The surface was then rinsed thoroughly with IPA to remove any excess FOTS and leave only a monolayer behind.

A solution of P3HpT in chloroform (7.5 mg mL^{-1}) were prepared and allowed to stir overnight. It was then filtered with 1 μm glass microfiber (GMF) filter immediately before being spin-coated onto FOTS passivated glass. The solution was spun at 300 rpm (250 rpm s^{-1} ramp) for 120 s, followed by 2000 rpm (1000 rpm s^{-1} ramp) for 30 s in ambient conditions. The films were dried under vacuum for 15 min to remove residual solvent and then transferred to PDMS after it had been oven cured.

5.3. Cyclic straining of samples

The thin film on elastomer samples (n = 7 for each strain) were mounted to a computer controlled linear actuator (before securing them, care was taken so that there was no sagging of the films). The samples were then strained and relaxed cyclically at either 5, 10, or 25%, up to 10000 cycles, with the absorption spectra measured before any strain cycles and after 1, 10, 20, 50, 100, 200, 500, 1000, 2000, 5000, and 10000 cycles.

5.4. UV–vis absorption spectroscopy

The absorbance of the materials was measured using an Agilent 8453 UV–vis spectrophotometer. The wavelength range measured was 850–300 nm with a step size of 1 nm. To account for the contribution to the absorption by PDMS, a strip of PDMS which had been subjected to the same conditions as the strained samples was used as a baseline for the absorption. The weakly interacting H-aggregate model was then used to perform a least squares fit to the absorption spectra between 550 and 620 nm (2.25 and 2.00 eV) using a Matlab program. The curves were initially normalized by setting the lowest point between 670 and 750 nm (1.85 and 1.65 eV) to zero [25] and then normalizing to the peak between 480 and 560 nm (2.58 and 2.21 eV). The proportion of aggregates in the film was determined only between 400 and 650 nm (3.10 and 1.91 eV). The choice of this range underestimated the fraction of amorphous material, but still allowed us to determine the general trend of the local ordering in the films.

5.5. Ductility measurements

After undergoing 10000 cycles of strain, samples of P3HpT on PDMS were strained 90% (the point at which pinhole cracks were observable in uncycled P3HpT on PDMS and just below the PDMS breaking point) and observed by optical microscopy. To compare to the behavior of a standard P3HpT film, samples of P3HpT on PDMS which had not been cyclically strained were also observed. The area occupied by cracks in the films was measured using Adobe Photoshop.

Acknowledgements

This work was supported by the Air Force Office of Scientific Research (AFOSR) Young Investigator Program, grant number FA9550-13-1-0156. Additional support was provided by the UC LEADS fellowship and the STARS Summer Research Program, awarded to A.S.-C. Chiang, the National Science Foundation Graduate Research Fellowship, awarded to S. Savagatrup, and by laboratory startup funds from the University of California, San Diego.

Appendix A. Supplementary data

Supplementary data associated with this article can be found, in the online version, at http://dx.doi.org/10.1016/j.synthmet.2016.03.033.

References

[1] R. Po, C. Carbonera, A. Bernardi, F. Tinti, N. Camaioni, Polymer- and carbon-based electrodes for polymer solar cells: toward low-cost, continuous fabrication over large area, Sol. Energy Mater. Sol. Cells 100 (2012) 97–114.
[2] N. Espinosa, M. Hösel, D. Angmo, F.C. Krebs, Solar cells with one-day energy payback for the factories of the future, Energy Environ. Sci. 5 (2012) 5117–5132.
[3] A. Anctil, C.W. Babbitt, R.P. Raffaelle, B.J. Landi, Cumulative energy demand for small molecule and polymer photovoltaics, Prog. Photovolt Res. Appl. 21 (2013) 1541–1554.
[4] F.C. Krebs, Fabrication and processing of polymer solar cells: a review of printing and coating techniques, Sol. Energy Mater. Sol. Cells 93 (2009) 394–412.
[5] P. Sommer-Larsen, M. Jørgensen, R.R. Søndergaard, M. Hösel, F.C. Krebs, Fast inline roll-to-roll printing for indium-tin-oxide-free polymer solar cells using automatic registration, Energy Technol. 1 (2013) 102–107.
[6] F.C. Krebs, N. Espinosa, M. Hösel, R.R. Søndergaard, M. Jørgensen, 25th anniversary article: rise to power—OPV-based solar parks, Adv. Mater. 26 (2014) 29–39.
[7] A.T. Yiu, P.M. Beaujuge, O.P. Lee, C.H. Woo, M.F. Toney, J.M.J. Fréchet, Side-chain tunability of furan-containing low-band-gap polymers provides control of structural order in efficient solar cells, J. Am. Chem. Soc. 134 (2012) 2180–2185.
[8] J. Mei, Z. Bao, Side chain engineering in solution-processable conjugated polymers, Chem. Mater. 26 (2014) 604–615.
[9] V. Brand, C. Bruner, R.H. Dauskardt, Cohesion and device reliability in organic bulk heterojunction photovoltaic cells, Sol. Energy Mater. Sol. Cells 99 (2012) 182–189.
[10] S.R. Dupont, M. Oliver, F.C. Krebs, R.H. Dauskardt, Interlayer adhesion in roll-to-roll processed flexible inverted polymer solar cells, Sol. Energy Mater. Sol. Cells 97 (2012) 171–175.
[11] D.J. Lipomi, H. Chong, M. Vosgueritchian, J. Mei, Z. Bao, Toward mechanically robust and intrinsically stretchable organic solar cells: evolution of photovoltaic properties with tensile strain, Sol. Energy Mater. Sol. Cells 107 (2012) 355–365.
[12] B.C.-K. Tee, C. Wang, R. Allen, Z. Bao, An electrically and mechanically self-healing composite with pressure- and flexion-sensitive properties for electronic skin applications, Nat. Nanotechnol. 7 (2012) 825–832.
[13] M. Kaltenbrunner, T. Sekitani, J. Reeder, T. Yokota, K. Kuribara, T. Tokuhara, M. Drack, R. Schwödiauer, I. Graz, S. Bauer-Gogonea, et al., An ultra-lightweight design for imperceptible plastic electronics, Nature 499 (2013) 458–463.
[14] S. Savagatrup, E. Chan, S.M. Renteria-Garcia, A.D. Printz, A.V. Zaretski, T.F. O'Connor, D. Rodriquez, E. Valle, D.J. Lipomi, Plasticization of PEDOT:PSS by common additives for mechanically robust organic solar cells and wearable sensors, Adv. Funct. Mater. 25 (2015) 427–436.
[15] D. Ghezzi, M.R. Antognazza, R. Maccarone, S. Bellani, E. Lanzarini, N. Martino, M. Mete, G. Perile, S. Bisti, G. Lanzani, et al., A polymer optoelectronic interface restores light sensitivity in blind rat retinas, Nat. Photonics 7 (2013) 400–406.
[16] M.L. Hammock, A. Chortos, B.C.-K. Tee, J.B.-H. Tok, Z. Bao, 25th anniversary article: the evolution of electronic skin (E-skin): a brief history, design considerations, and recent progress, Adv. Mater. 25 (2013) 5997–6038.
[17] S.C.B. Mannsfeld, B.C.-K. Tee, R.M. Stoltenberg, C.V.H.-H. Chen, S. Barman, B.V. O. Muir, A.N. Sokolov, C. Reese, Z. Bao, Highly sensitive flexible pressure sensors with microstructured rubber dielectric layers, Nat. Mater. 9 (2010) 859–864.
[18] D.J. Lipomi, M. Vosgueritchian, B.C.-K. Tee, S.L. Hellstrom, J.A. Lee, C.H. Fox, Z. Bao, Skin-like pressure and strain sensors based on transparent elastic films of carbon nanotubes, Nat. Nanotechnol. 6 (2011) 788–792.
[19] M. Jørgensen, K. Norrman, F.C. Krebs, Stability/degradation of polymer solar cells, Sol. Energy Mater. Sol. Cells 92 (2008) 686–714.
[20] M. Jørgensen, K. Norrman, S.A. Gevorgyan, T. Tromholt, B. Andreasen, F.C. Krebs, Stability of polymer solar cells, Adv. Mater. 24 (2012) 580–612.
[21] F.C. Krebs, T.D. Nielsen, J. Fyenbo, M. Wadstrøm, M.S. Pedersen, Manufacture, integration and demonstration of polymer solar cells in a lamp for the lighting africa initiative, Energy Environ. Sci. 3 (2010) 512–525.
[22] F.C. Spano, Modeling disorder in polymer aggregates: the optical spectroscopy of regioregular poly(3-hexylthiophene) thin films, J. Chem. Phys. 122 (2005) 234701.
[23] J. Clark, J.-F. Chang, F.C. Spano, R.H. Friend, C. Silva, Determining exciton bandwidth and film microstructure in polythiophene films using linear absorption spectroscopy, Appl. Phys. Lett. 94 (2009) 163306.
[24] S.T. Turner, P. Pingel, R. Steyrleuthner, E.J.W. Crossland, S. Ludwigs, D. Neher, Quantitative analysis of bulk heterojunction films using linear absorption spectroscopy and solar cell performance, Adv. Funct. Mater. 21 (2011) 4640–4652.
[25] O. Awartani, B.I. Lemanski, H.W. Ro, L.J. Richter, D.M. DeLongchamp, B.T. O'Connor, Correlating stiffness, ductility, and morphology of polymer: fullerene films for solar cell applications, Adv. Energy Mater. 3 (2013) 399–406.

[26] A.D. Printz, A.V. Zaretski, S. Savagatrup, A.S.-C. Chiang, D.J. Lipomi, Yield point of semiconducting polymer films on stretchable substrates determined by onset of buckling, ACS Appl. Mater. Interfaces 7 (2015) 23257–23264.
[27] S. Savagatrup, A.D. Printz, D. Rodriquez, D.J. Lipomi, Best of both worlds: conjugated polymers exhibiting good photovoltaic behavior and high tensile elasticity, Macromolecules 47 (2014) 1981–1992.
[28] S. Savagatrup, A.D. Printz, H. Wu, K.M. Rajan, E.J. Sawyer, A.V. Zaretski, C.J. Bettinger, D.J. Lipomi, Viability of stretchable poly(3-heptylthiophene) (P3HpT) for organic solar cells and field-effect transistors, Synth. Met. 203 (2015) 208–214.
[29] J.-S. Kim, J.-H. Kim, W. Lee, H. Yu, H.J. Kim, I. Song, M. Shin, J.H. Oh, U. Jeong, T.-S. Kim, et al., Tuning mechanical and optoelectrical properties of poly(3-hexylthiophene) through systematic regioregularity control, Macromolecules 48 (2015) 4339–4346.
[30] F.C. Spano, Absorption in regio-regular poly(3-hexyl)thiophene thin films: fermi resonances, interband coupling and disorder, Chem. Phys. 325 (2006) 22–35.
[31] G. Louarn, M. Trznadel, Raman spectroscopic studies of regioregular poly (3-alkylthiophenes), J. Phys. Chem. 3654 (1996) 12532–12539.
[32] P. Pingel, A. Zen, R.D. Abellón, F.C. Grozema, L.D.A. Siebbeles, D. Neher, Temperature-resolved local and macroscopic charge carrier transport in thin P3HT layers, Adv. Funct. Mater. 20 (2010) 2286–2295.
[33] N. Bowden, S. Brittain, A.G. Evans, J.W. Hutchinson, G.M. Whitesides, Spontaneous formation of ordered structures in thin films of metals supported on an elastomeric polymer, Nature 393 (1998) 146–149.
[34] C.M. Stafford, C. Harrison, K.L. Beers, A. Karim, E.J. Amis, M.R. VanLandingham, H.-C. Kim, W. Volksen, R.D. Miller, E.E. Simonyi, A buckling-based metrology for measuring the elastic moduli of polymeric thin films, Nat. Mater. 3 (2004) 545–550.
[35] C.M. Stafford, B.D. Vogt, C. Harrison, D. Julthongpiput, R. Huang, Elastic moduli of ultrathin amorphous polymer films, Macromolecules 39 (2006) 5095–5099.
[36] D. Tahk, H.H. Lee, D.-Y. Khang, Elastic moduli of organic electronic materials by the buckling method, Macromolecules 42 (2009) 7079–7083.